Available online at www.sciencedirect.com
SCIENCE DIRECT
Journal of Catalysis 229 (2005) 424–438
JOURNAL OF CATALYSIS
www.elsevier.com/locate/jcat

The effect of glycol on phosphate-doped CoMo/Al_2O_3 hydrotreating catalysts

Daniele Nicosia, Roel Prins *

Institute of Bioengineering, Federal Institute of Technology (ETH), 8093 Zurich, Switzerland

Received 6 July 2004; revised 1 October 2004; accepted 4 November 2004

Available online 24 December 2004

Abstract

γ-Al_2O_3-supported CoMo catalysts doped with phosphate and prepared in the presence of triethylene glycol (TEG), ethylene glycol (EG), and triethylene dimethyl ether (TEG-DME) were tested in the hydrodesulfurization (HDS) of thiophene. The catalyst containing TEG showed a higher catalytic activity than the catalyst prepared without TEG. Laser Raman spectroscopy and EXAFS demonstrated that the impregnation solution containing the metal salts and phosphoric acid contained $HP_2Mo_5O_{23}^{5-}$ diphosphopentamolybdate and that this anion was not affected by the presence of TEG. ^{31}P NMR measurements of the impregnation solution showed a paramagnetic effect of cobalt, which proved that cobalt is complexed by the diphosphopentamolybdate, both in the presence and absence of TEG. DRIFT experiments with a γ-Al_2O_3 support treated with TEG proved that glycol interacts with the basic OH_s groups and coordinatively unsaturated Al^{3+} sites. The diphosphopentamolybdate complexes are decomposed by these sites on the γ-Al_2O_3 support, but EXAFS of the dried catalyst precursor showed that in the presence of glycol this decomposition was partially prevented. This favored the precipitation in the alumina pores of clusters in which Co and Mo are in close proximity. Because of their high Co/Mo atomic ratio, these complexes lead to an efficient decoration of the MoS_2 slabs by the promoter atoms during the sulfiding treatment, thus increasing the catalytic performance of the supported CoMo catalyst.

Keywords: Triethylene glycol; Ethylene glycol; Triethylene glycol dimethyl ether; Phosphomolybdate species; CoMo HDS catalysts; EXAFS; Paramagnetic effect of cobalt on ^{31}P NMR; Laser Raman spectroscopy

1. Introduction

Cobalt (or nickel) and molybdenum sulfides are extensively used in refineries as hydrotreating catalysts to remove sulfur and nitrogen from oil fractions. Molybdenum sulfide is considered to be the actual catalyst and cobalt sulfide the promoter. The removal of sulfur and nitrogen is extremely important because their noxious oxides are released in automotive gas exhaust. As laws concerning the control of atmospheric pollutants are becoming stricter, it is necessary to improve the hydrotreating activity of these types of catalysts.

A hydrotreating catalyst is usually prepared by the impregnation of a silica or γ-Al_2O_3 support with an aqueous solution of cobalt (or nickel) and molybdenum salts. The dried powder is calcined at an elevated temperature, and a further sulfidation treatment converts the oxidic precursors into the catalytically active sulfides. A new way of preparing more active hydrodesulfurization (HDS) catalysts is to add phosphate and a glycol to the impregnating solution [1]. Phosphate has the beneficial effect of increasing the solubility of the molybdenum salts and the stability of the impregnation solution. Without the addition of phosphate, a light orange or green precipitate is often observed within a few minutes after each metallic salt is dissolved in the preparation of Co + Mo or Ni + Mo impregnation solutions [2]. A promotional effect of phosphate on HDN, especially when the hydrogenation of aro-

* Corresponding author. Fax: +41-1-6321162.
E-mail address: roel.prins@chem.ethz.ch (R. Prins).

0021-9517/$ – see front matter
doi:10.1016/j.jcat.2004.11.014

matic rings is the rate-determining step, has also been reported [3]. When phosphate is added to the impregnation solution, it reacts with the molybdenum precursor and, depending on the reaction conditions, gives rise to a variety of phosphomolybdate anions, such as Keggin ($PMo_{12}O_{40}^{3-}$, $PMo_{12}O_{40}^{7-}$), Dawson ($P_2Mo_{18}O_{62}^{6-}$), and diphosphopentamolybdate ($P_2Mo_5O_{23}^{6-}$) anions [4,5]. Depending on the structure of the phosphomolybdate anions, the cobalt or nickel promoter can stay in solution as a solvated aquocomplex or become complexed by the phosphomolybdate. Cobalt diphosphopentamolybdates ($Co_xH_{(6-2x)}P_2Mo_5O_{23}$) have a higher Co/Mo atomic ratio than salts of the Keggin or Dawson anions. Griboval et al. reported that the use of $Co_xH_{(6-2x)}P_2Mo_5O_{23}$ as a catalyst precursor favors a higher Co/Mo atomic ratio in the final sulfided catalyst and thus improves the promotion of the active phase because a better decoration of the cobalt on the MoS_2 edge is obtained [6,7]. The adsorption of phosphomolybdates on a support was described extensively by several authors. For instance, van Veen et al. reported that upon adsorption on γ-Al_2O_3 the $P_2Mo_5O_{23}^{6-}$ ion decomposes into $AlPO_4$ and molybdate [8], whereas Cheng and Luthra reported that the $PMo_{12}O_{40}^{3-}$ ion adsorbs intact [9].

Chelating ligands like nitriloacetic acid (NTA) and ethylene diamine tetraacetic acid (EDTA) are also used as additives, instead of phosphate, to improve the catalytic activity of hydrotreating catalysts [10]. By means of Quick EXAFS measurements on NiMo/SiO_2, Cattaneo et al. observed that these organic ligands complex nickel rather than molybdenum [11,12]. The beneficial effect of the chelating ligands was explained by a retardation of the sulfidation of the nickel cations while molybdenum is being fully sulfided. Moreover, by weakening the nickel–support interactions, the chelating ligands increase the mobility of the nickel on the support so that the promoter can more easily reach the MoS_2 phase, thus favoring the formation of the catalytically active Ni–Mo–S phase [11]. Why glycol has a positive effect on the catalytic activity has not been elucidated yet. As promotion by chelating is very unlikely for glycols, because they are known to have only weak chelating properties, we wanted to obtain insight into the role of these molecules in the catalytic activity of the CoMo catalysts and to investigate whether and how glycol is aided by phosphate. By means of several techniques, we mainly studied the role of triethylene glycol to elucidate whether, despite its weak chelating activity, the effect of this organic polyglycol resembles that of NTA or EDTA.

2. Experimental

2.1. Sample preparation and characterization

The wet impregnation method was used to prepare catalysts supported with CoMoP, CoMoP-EG (containing ethylene glycol, EG), CoMoP-TEG (containing triethylene glycol, TEG), and CoMoP-TEG-DME (containing triethylene glycol dimethyl ether, TEG-DME), according to the European patent application 0601722 B1 [1]. In short, 2.7 g of MoO_3 powder (18.7 mmol, Fluka, purum, p.a.) and 0.5 ml of an 85 wt% aqueous H_3PO_4 solution (7.5 mmol H_3PO_4, Aldrich, p.a.) were dissolved in 10 ml of water under stirring and refluxed at 80 °C for one night. The solution was cooled to room temperature, 1 g of $CoCO_3$ (8.5 mmol, Aldrich p.a.) was added, and the solution was stirred for 3 h; upon the addition of the cobalt salt, the evolution of CO_2 was observed. The color of the resulting solution was red and the pH was 3.0. After $CoCO_3$ had dissolved, we added 0.8 ml of EG (15 mmol, Aldrich, p.a.) for the preparation of the CoMoP-EG solution, 2 ml of TEG (15 mmol, Aldrich, p.a.) for the CoMoP-TEG, and 2 ml of TEG-DME (11.2 mmol, Fluka, purum, p.a.) for the preparation of the CoMoP-TEG-DME solution. No changes in pH or color were observed after the addition of the glycols. MgMoP and MgMoP-TEG reference solutions were prepared as described for the corresponding Co-containing solutions, with 0.6 g $Mg_5(CO_3)_4(OH)_2 \cdot 5H_2O$ (1.2 mmol, Aldrich p.a.) and the same amount of MoO_3 powder, H_3PO_4 solution, and TEG as mentioned above.

Two catalysts, CoMoP_std and CoMoP-TEG_std, were prepared by dissolving at room temperature 3.26 g of $(NH_4)_6Mo_7O_{24} \cdot 4H_2O$ (2.6 mmol, Fluka purum p.a.) and 0.5 ml of 85 wt% aqueous H_3PO_4 solution in 10 ml of distilled water. After the heptamolybdate salt had dissolved, the solution turned yellowish. Then, 2.32 g of $Co(NO_3)_2 \cdot 6H_2O$ (8.0 mmol, Fluka, purum p.a.) was added and, in the case of the CoMoP-TEG_std solution, 2 ml of TEG was added afterward. The color of the resulting solutions was red, but after about 24 h, precipitation of orange crystals was observed. We also prepared CoMo-TEG- and CoMo-supported catalysts, by following the classical method described by Medici and Prins [13]. MoO_3 (2.7 g) was dissolved with stirring at room temperature in 10 ml of 25% aqueous NH_3 solution. When the MoO_3 was dissolved, 2.5 g $Co(NO_3)_2 \cdot 6H_2O$ was added. The color of the solution was red. In the case of the CoMo-TEG impregnation solution, 2 ml TEG (Fluka, purum, p.a.) was added; the final pH of the solution was 9 for both the CoMo and CoMo-TEG impregnation solutions.

Prior to impregnation with one of the impregnating solutions, the SiO_2 (C560 Chemie Uetikon), γ-Al_2O_3 (Condea Chemie), and a γ-Al_2O_3 support impregnated with 0.8 ml of a 20% aqueous and TEG acidic solution (pH 2.5 by means of HCl 35%; J.T. Baker) were crushed, sieved to a grain size of 90–125 mm, and dried overnight in an oven at 120 °C. The idea behind adding HCl to the TEG solution was to obtain the same pH value as the original CoMoP and CoMoP-TEG solution. In this way, the absorption of TEG on the γ-Al_2O_3 support was not affected by a different charge on the alumina surface. The total water pore volumes of the SiO_2, γ-Al_2O_3, and γ-Al_2O_3 + TEG were 0.8, 0.9, and 0.4 ml/g, respectively. Therefore, during the impregnation of dried

Table 1
Hydrotreating doped catalysts

Catalyst	Loading (wt%)			Co/Mo mol ratio	P/Mo mol ratio	BET s.a. (m^2/g)	P.V. (cm^3/g)	Av. P.D. (nm)	Conversion/(Co + Mo) (g^{-1})
	Mo	Co	P						
CoMo/γ-Al_2O_3	12.30	2.60	–	0.34	–	115	0.25	5.8	1.6
CoMo-TEG/γ-Al_2O_3	12.40	2.49	–	0.31	–	90	0.21	5.3	1.7
CoMoP/γ-Al_2O_3	12.85	2.88	1.75	0.37	0.42	144	0.32	6.3	2.4
CoMoP-EG/γ-Al_2O_3	12.84	2.37	1.91	0.30	0.46	97	0.25	6.4	2.7
CoMoP-TEG/γ-Al_2O_3	12.47	2.86	1.60	0.37	0.40	114	0.28	5.7	2.8
CoMoP/γ-Al_2O_3 + TEG	10.71	2.64	1.51	0.40	0.44	101	0.20	5.6	2.3
CoMoP_std/γ-Al_2O_3	10.90	2.40	1.40	0.36	0.40	128	0.28	6.0	2.0
CoMoP_std-TEG/γ-Al_2O_3	9.80	1.90	1.50	0.32	0.47	127	0.27	5.3	2.4
CoMoP-TEG-DME/γ-Al_2O_3	11.73	1.99	1.50	0.28	0.40	110	0.25	5.3	2.0
CoMoP/SiO_2	9.20	2.20	1.35	0.39	0.45	350	0.57	4.9	0.5
CoMoP-TEG/SiO_2	9.76	2.39	1.50	0.40	0.48	207	0.36	4.7	0.3
γ-Al_2O_3 + TEG	–	–	–	–	–	160	0.35	5.3	–
γ-Al_2O_3 + TEG-DME	–	–	–	–	–	172	0.37	5.4	–
γ-Al_2O_3 + EG	–	–	–	–	–	192	0.38	5.3	–
γ-Al_2O_3	–	–	–	–	–	210	0.45	6.0	–
SiO_2	–	–	–	–	–	469	0.81	4.7	–

SiO_2 and γ-Al_2O_3, we used 0.8 and 0.9 ml of impregnation solution, respectively. However, when impregnating the γ-Al_2O_3 + TEG support with about 0.9 ml of impregnation solution, we observed the formation of lumps. This was due to the excess of solution that did not fit in the pore volume of that support. Nevertheless, as we wanted to compare the performance of a CoMoP catalyst prepared with the γ-Al_2O_3 + TEG support with the performance of the other catalysts, we had to use the same metal loading. Since it was impossible to prepare a more concentrated impregnation solution, the only alternative was to use a double impregnation. Therefore the γ-Al_2O_3 + TEG support was double impregnated with 0.4 ml of impregnation solution, to obtain about the same metal loading of the other catalyst precursors.

We also prepared γ-Al_2O_3 + EG and γ-Al_2O_3 + TEG-DME samples by impregnating the γ-Al_2O_3 with 0.8 ml of a 20% aqueous and EG acidic solution (pH 2.5 by means of HCl 35%). After impregnation, the wet powder was dried overnight at 120 °C with a heating ramp of 2 °C/min. All catalysts were prepared without calcination. The investigated catalyst precursors are listed in Table 1. Atomic absorption spectroscopy was performed with a Varian SpectraAA 200FS atomic absorption spectrometer, equipped with a hollow tube lamp for the absorption of Co and Mo at 240.7 and 313.3 nm, respectively. The measurements were carried out with a slit of 0.1 nm and a lamp current of 7 mA. The flame was oxidizing (acetylene + air) for the measurement of Co and reducing (acetylene + nitrous oxide) for the measurement of Mo. For the measurements of the phosphorus content, a photometric method was employed. The sample was dissolved and a certain amount of ligand was added that bound phosphate only, forming a colored complex. By measuring the UV–vis absorbance of this phosphate-complex, we obtained the amount of phosphorus in the sample.

Nitrogen adsorption measurements of the dried but not calcined samples were performed at liquid-nitrogen temperature with a Micromeritics TriStar 3000 apparatus. Prior to the measurement, the samples were degassed at 200 °C at 10 Pa for one night to prevent the decomposition of the organic compounds. For the measurements of the SiO_2 and γ-Al_2O_3 supports, the degassing was carried out at 400 °C. Because no calcination was performed, the BET surface area of the CoMo/γ-Al_2O_3 catalysts was only 115 m^2/g, whereas the calcined CoMo/γ-Al_2O_3 showed a BET surface area of 177 m^2/g. The surface area was determined from the nitrogen adsorption isotherm according to the BET method, and the pore size distribution was determined from the desorption branch of the isotherm according to the BJH method. Raman measurements were performed on a Bruker Equinox 55 spectrometer equipped with a FT-Raman-Module FRA 106/S, with a Nd:YAG laser (1064 nm, 400 mW), a CaF_2 beam-splitter, and a Ge detector (D418-S) cooled by liquid nitrogen. About 2 ml solution was used for the measurements. For the Raman experiments on the dried catalyst precursors, the powder was pressed in an aluminum disk. The number of accumulated spectra for each sample was 4096. ^{31}P NMR spectra were acquired on a Bruker AMX400 spectrometer at a magnetic field of 9.4 T and a resonance frequency of 161.98 MHz. For each spectrum 32 scans were acquired. The chemical shift was referenced to 85% phosphoric acid (0 ppm). UV–vis diffuse reflectance measurements were performed on a Varian Cary 3 spectrophotometer equipped with a diffuse reflectance cell. The measurements were scanned against a pure $BaSO_4$ background. DRIFT measurements were performed on a BioRad "excalibur" FTIR equipped with a Spectra Tech Inc. DRIFT cell. The measurements were carried out at 150 °C and flushing with helium to evaporate the adsorbed water and CO_2 from the sample. For each measurement 128 scans were

collected, and no further treatment of DRIFT spectra was performed.

2.2. Sulfidation and reaction

We used a modified version of the setup described in [14] to perform the sulfidation and catalytic tests at atmospheric pressure. The oxidic precursor (0.1 g) was diluted in 0.9 g of SiC and sulfided at 400 °C (heating rate 6 °C/min) for 2 h with a mixture of 10% H_2S in H_2 (Messer Griesheim 3.0). The sulfiding mixture flowed through the reactor at 60 ml/min from the beginning of the heating process. The reactor consisted of a quartz tube (inner diameter 13 mm, outer diameter 16 mm, length 350 mm) equipped with a quartz frit in the middle. The activity of all catalysts was tested in the HDS of thiophene at 350 °C [13]. We obtained the feed, consisting of 3% thiophene in H_2, by bubbling H_2 through a series of four thiophene saturators that were cooled to 2 °C. The thiophene/H_2 mixture flowed over the catalyst at 75 ml/min, corresponding to a GHSV of 22000 h^{-1}. The flow rates of H_2S and H_2 were regulated with Brooks thermal mass flow controllers. The product stream was analyzed on line with a Varian CG3600C gas chromatograph, with the use of a WCOT fused silica 0.25 mm ×50 m capillary column with a CP-SIL5CB coating; data were collected every 12 min. A flame ionization detector (FID) was used to analyze the composition of the outcoming gas. The sample was injected into the column by means of a six-way valve and a 150-μl loop. The temperature of the column was kept constant at 40 °C until the products of hydrodesulfurization (in order of appearance: 1-butane, *n*-butane, *trans*-2-butene, and *cis*-2-butene) were detected; then the temperature was quickly raised to 70 °C and the thiophene peak was finally detected. The results, obtained 3.5 h after the first measurement, were used to estimate the thiophene conversion of the catalysts. The conversion of all catalysts was normalized for the Co + Mo loading of the oxidic catalyst precursor, to directly compare catalysts with a slightly different metal loading.

2.3. EXAFS data collection and analysis

EXAFS spectra of the investigated compounds were measured at the Mo *K*-edge. Data were collected at the Swiss Norwegian Beamline (SNBL, BM01) at the European Synchrotron Radiation Facility (ESRF) in Grenoble, France. The energy of the ring was 6 GeV, and the current was 200 mV. Details regarding the beamline setup and the method of acquiring EXAFS data were published previously [11]. The samples were mixed with graphite, pressed into self-supporting wafers, and mounted in an in situ cell [15]. The thickness of the samples was adapted to an overall X-ray absorption of $\mu x = 1$. All samples were cooled to liquid nitrogen temperature during the measurements.

The program XDAP (version 2.3.3) was used for the fit analysis of the data [16]. The background removal was carried out according to the method described by Koningsberger et al. [17]. Normalization was done by dividing the absorption intensities of three averaged data scans by the height of the absorption edge and subtracting the background with the use of a cubic spline routine. For the analysis of the Mo–O, Mo–Mo, and Mo–P contributions, EXAFS data from experimental reference compounds were used. The following compounds were used: Na_2MoO_4 for the Mo–O contribution, MoS_2 for the Mo–Mo contribution, and MoP for the Mo–P contribution. For other Mo-X contributions, the FEFF 8 code [18] was used to generate theoretical references. MoP was prepared by direct reduction of amorphous molybdenum phosphate [19]. The calibration of the references was carried out as described in [20]. Like the EXAFS spectra of the catalysts, the reference spectra were measured at liquid nitrogen temperature; thus the references were optimized for the data analysis.

Data analysis was performed by multiple shell fits in *R* space. P and Co backscatterers were identified by application of the difference file technique with phase-corrected Fourier transforms [17]. Each fit was performed with the k^0 and k^1 weight factors to check for the correctness of the fit [21]. The errors in the structural parameters were calculated from the covariance matrix, taking into account the statistical noise of the EXAFS data and the correlation between the different coordination parameters. The number of independent data points was calculated as reported in the "Reports on Standards and Criteria in XAFS Spectroscopy" [22]. The variances of the magnitude and imaginary parts of the Fourier transform of the fitted and the experimantal data were calculated according to the equation

$$k^n \text{ variance} = \frac{\int [k^n (FT_{\text{model}}(R) - FT_{\text{EXP}}(R))]^2 \mathrm{d}R}{\int [k^n FT_{\text{EXP}}(R)]^2 \mathrm{d}R}.$$

The quality of the fit was also estimated from the value of the goodness of the fit. This value takes the number of free parameters into account and is used to determine whether the addition of new parameters makes sense; a small value of the goodness means a good fit.

3. Results

3.1. Catalytic test

The activities of the CoMo catalysts prepared according to different routes show that the CoMo/γ-Al_2O_3 and CoMo-TEG/γ-Al_2O_3 catalysts gave almost the same thiophene conversion (Table 1) at 350 °C and GHSV = 22000 h^{-1}, 3.5 h after the first measurement. This indicates that TEG has almost no influence on the HDS activity of a CoMo catalyst prepared according to the standard route. Phosphate has a beneficial effect because the CoMoP/γ-Al_2O_3 catalyst showed a higher conversion than the catalysts prepared without phosphoric acid. However, when we used glycols and phosphoric acid, as we did for the CoMoP-EG/γ-Al_2O_3 and

CoMoP-TEG/γ-Al_2O_3 catalysts, the conversion was even higher. These results show that there is a synergistic effect between phosphate and glycol.

However, the catalytic activity of the CoMoP/γ-Al_2O_3 + TEG sample was lower than that of the CoMoP-TEG/γ-Al_2O_3 and CoMoP-EG/γ-Al_2O_3 catalysts. The double-impregnation method that was employed for the preparation of this catalyst may have led to a bad dispersion of the catalyst, thus causing a decrease in activity.

The promoting effect of phosphate is shown as well for the CoMoP_std/γ-A_2O_3 catalyst, which showed a higher activity than the catalysts prepared without phosphoric acid. Moreover, a higher conversion is observed for CoMoP-TEG_std/γ-A_2O_3, showing that TEG has a positive effect on the catalytic activity even when a standard route of preparation is used. Despite the presence of phosphate and glycol, CoMoP-TEG_std/γ-A_2O_3 showed a lower activity than CoMoP-TEG/γ-A_2O_3. The CoMoP-TEG-DME/γ-Al_2O_3 catalyst also showed a lower activity, although it was prepared in the presence of both phosphoric acid and glycol. As far as the silica-supported catalysts are concerned, a very poor catalytic activity was obtained.

3.2. Characterization of the impregnation solution

3.2.1. Laser Raman spectroscopy

Fig. 1 shows the laser Raman spectra of the impregnation solutions of CoMoP and CoMoP-TEG and of an aqueous solution of TEG. All of the spectra show a common feature at about 3250 cm^{-1} arising from water. The CoMoP solution showed two peaks at 940 and 890 cm^{-1}, which are typical for the $HP_2Mo_5O_{23}^{5-}$ anion [23,24]. This anion has a structure consisting of five interconnected octahedral MoO_6 units surrounding two PO_4 tetrahedrons. No bands of free phosphate or molybdate species were observed. This is in good agreement with the stoichiometric amount of molybdenum and phosphate in the impregnation solution. In addition to these two peaks, signals at 2948, 2886, and 1466 cm^{-1} were observed in the CoMoP-TEG spectrum. These signals arise from the CH stretching, CH_2 scissoring, and CH_2 twisting vibration of the TEG molecule. The bands at 940 and 890 cm^{-1} indicate that the $HP_2Mo_5O_{23}^{5-}$ anion is formed in the CoMoP-TEG impregnation solution as well. Judging from the small shoulder at 830 cm^{-1}, assigned to the stretching vibration of the C–O unit of TEG, the 888 cm^{-1} TEG band is hidden under the 890 cm^{-1} bands from the $HP_2Mo_5O_{23}^{5-}$ anion. Raman spectra for the CoMoP_std and CoMoP_std-TEG (not shown here) were recorded as well and showed the same results.

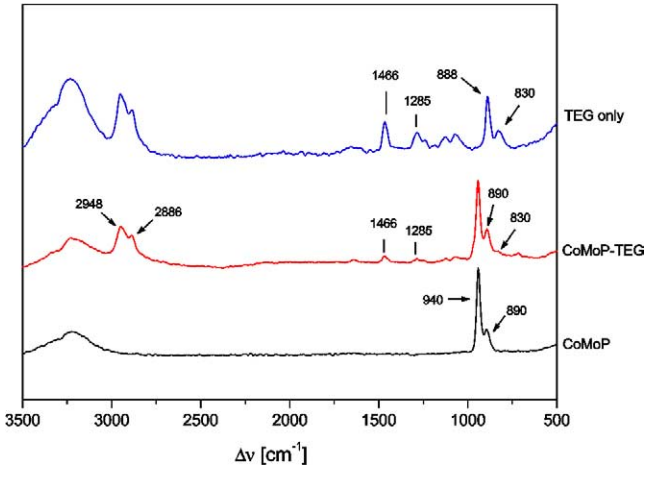

Fig. 1. Laser Raman spectra of the CoMoP impregnation solution prepared in the presence and absence of TEG and of an aqueous solution of TEG.

3.2.2. ^{31}P and ^{13}C NMR

The ^{31}P NMR spectrum of the CoMoP-TEG impregnation solution shows a very broad peak with a maximum at about 50 ppm and three sharp peaks between −2 and −4 ppm (Fig. 2). The broadening and shifting of the NMR signals are due to the paramagnetic effect of the cobalt cations on the ^{31}P nuclei. Because of their high magnetic moment, paramagnetic cobalt ions decrease the relaxation time of phosphorus strongly. As a consequence, the ^{31}P NMR peaks are broadened. The peaks are also shifted in proportion to the electron density of Co^{2+} on the ^{31}P nucleus. Therefore, the higher the number of Co ions around a P atom is, the stronger the paramagnetic effect is [25]. Although the paramagnetic effect of cobalt did not allow us to determine which phosphomolybdate ions are present in solution, it indicates that cobalt and phosphorus are in close proximity. Harris et al. made use of paramagnetic cobalt to probe the phosphate binding in the Co^{2+}-substituted derivative of the *Streptomyces dizinc aminopeptidase* enzyme [26]. Adding Co^{2+} ions to a solution of this enzyme, they observed that as soon as cobalt replaced zinc, the phosphorus NMR signal became very broad. That proved the close interaction between cobalt and phosphorus. ^{31}P NMR spectra of the MgMoP and MgMoP-TEG impregnation solutions (not shown here) allowed us to assign the phosphomolybdate species. Both spectra showed one strong signal at 2.1 ppm that is typical for the $HP_2Mo_5O_{23}^{5-}$ ion [27]. The spectra also showed a pair of small signals at around 0 ppm. These signals may arise from small amounts of $PMo_{11}O_{39}^{7-}$ and $PMo_9O_{31}(OH)_3^{7-}$ [27]. Similarly, we believe that small amounts of these compounds gave rise to the sharp peaks in the ^{31}P NMR spectra of the CoMoP (not shown) and CoMoP-TEG solutions as well (Fig. 2). The presence of TEG did not affect the formation of the $HP_2Mo_5O_{23}^{5-}$ anion. Moreover, ^{13}C NMR carried out on the CoMoP-TEG impregnation solution showed three sharp signals (not shown here) corresponding to the C–OH (60 ppm), COC (70 ppm), and CH_2 (72 ppm) carbon atoms of the isolated TEG. TEG was not in close proximity to Co^{2+} ions, demonstrating that, as expected, TEG did not form chelates with Co^{2+} ions.

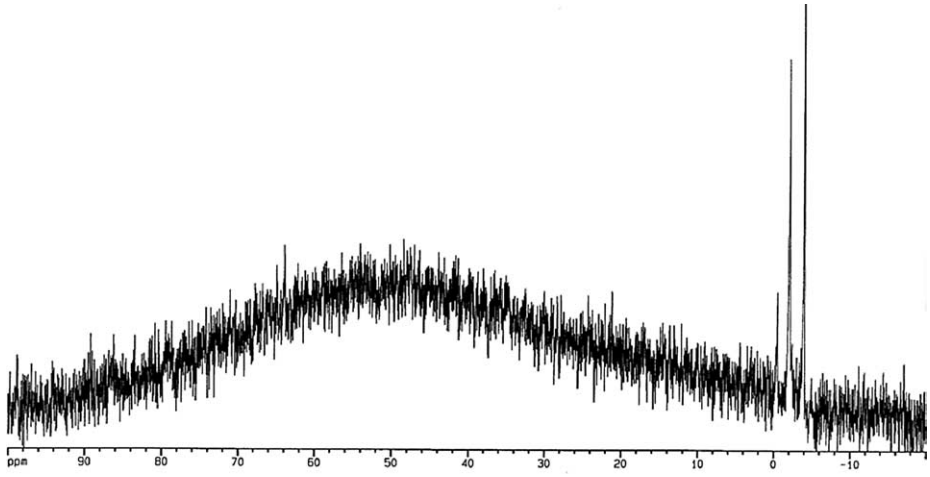

Fig. 2. ^{31}P NMR spectra of the CoMoP impregnation solution prepared in the presence of TEG.

3.2.3. Mo K-edge EXAFS

In Fig. 3 the k^3-weighted EXAFS functions are presented that were derived from the Mo K-edge EXAFS spectra of the CoMoP and CoMoP-TEG impregnation solutions. They show that the presence of TEG does not affect the local environment of the molybdenum. Therefore, we performed an EXAFS analysis of the CoMoP impregnation solution only. Fig. 4 shows that a fit with three Mo–O contributions, one Mo–Mo contribution, and one Mo–P contribution describes the experimental results very well between 0.5 and 4 Å. Fig. 5 shows that the Fourier transform of the fitted Mo–P contribution agrees very well with the Fourier transform of the corresponding difference file in both k^1 and k^3 weighting. The resulting parameters of the EXAFS data analysis for the CoMoP impregnation solution are listed in Table 2. The variances of the fits of the imaginary and absolute parts of the Fourier transform were close to 1%, indicating a high-quality fit. The results of the fit show that the distances and coordination numbers of the Mo–Mo and Mo–P shells correspond to the $HP_2Mo_5O_{23}{}^{5-}$ anion [28]. This confirms the Raman and ^{31}P NMR measurements.

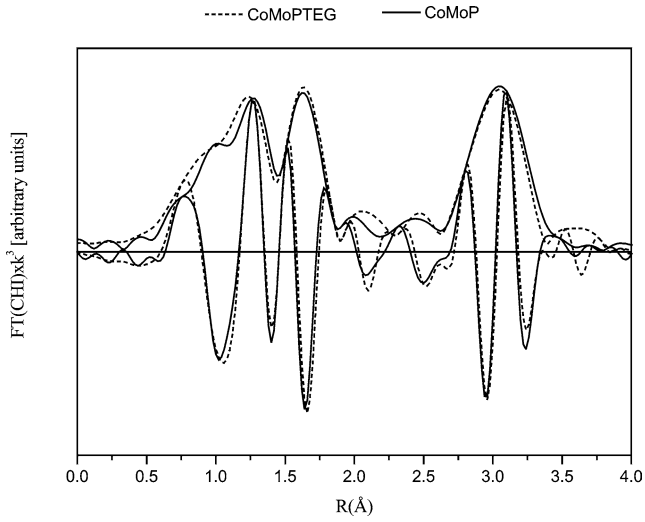

Fig. 3. Mo K-edge k^2-weighted EXAFS Fourier transforms of the CoMoP impregnation solution prepared in the presence (dashed) and absence (solid) of TEG.

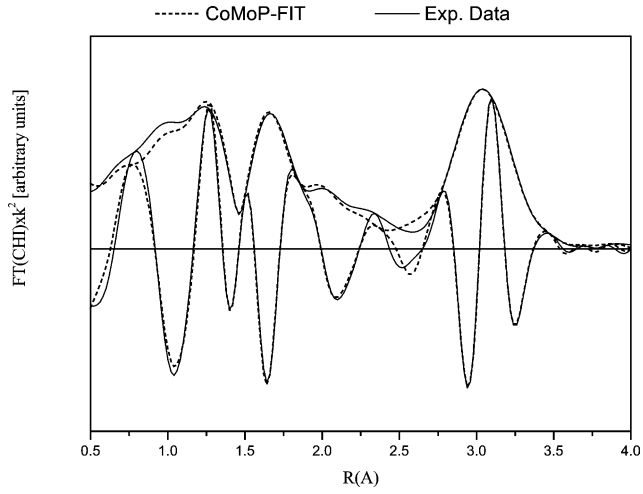

Fig. 4. Mo K-edge k^2-weighted EXAFS Fourier transforms of the CoMoP impregnation solution, experimental (solid) and fit (dashed). $\Delta k = 4.8$–16.5 Å^{-1}, $\Delta R = 0.5$–4 Å.

3.3. Characterization of the dried catalyst precursors

3.3.1. UV–visible diffuse reflectance and Raman spectroscopy

Ultraviolet–visible diffuse reflectance spectra for the CoMoP/SiO_2, CoMoP-TEG/γ-Al_2O_3, CoMoP_std-TEG/γ-Al_2O_3, CoMoP/γ-Al_2O_3 + TEG, CoMoP-TEG-DME/γ-Al_2O_3, CoMoP_std/γ-Al_2O_3, and CoMoP/γ-Al_2O_3 samples are shown in Fig. 6. All of the samples showed a broad band centered at around 225 nm. According to Fournier et al. and William et al., this band is common to both tetrahedrally and octahedrally coordinated molybdenum [29–31]. A much broader signal centered at 325 nm was observed for CoMoP/SiO_2, CoMoP-TEG/γ-Al_2O_3, CoMoP_std-TEG/γ-Al_2O_3, and CoMoP/γ-Al_2O_3 + TEG. This signal is typical for octahedrally coordinated molybdenum and was also

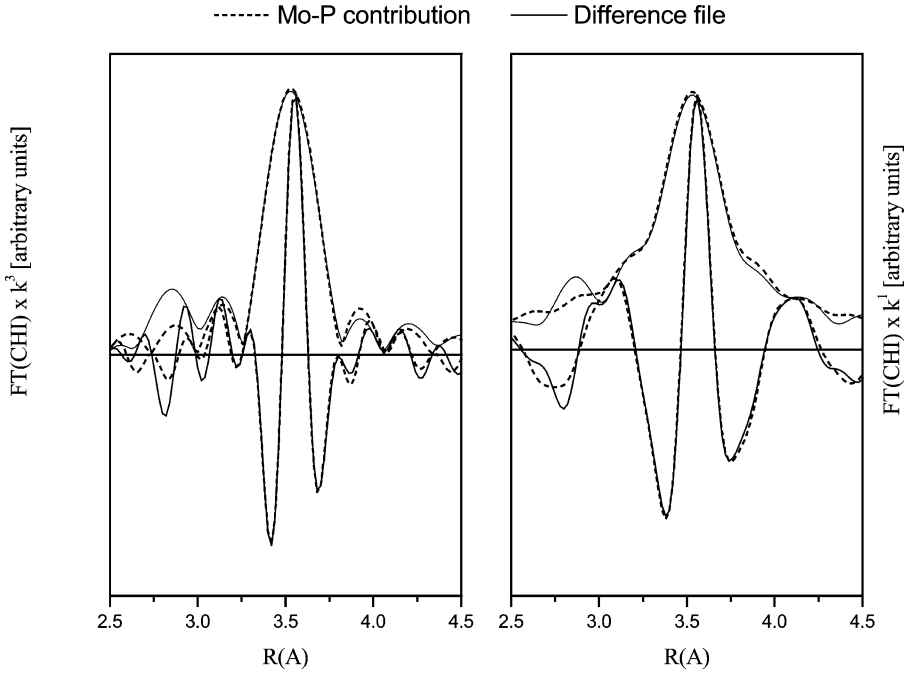

Fig. 5. k^1 (right) and k^3 (left) weighted EXAFS Fourier transforms of the fitted Mo–P contribution in the CoMoP impregnation solution (dotted) and difference file (solid).

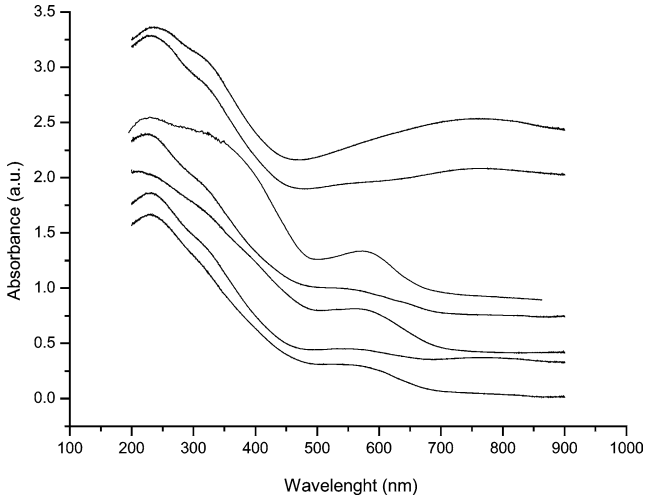

Fig. 6. Reflectance UV–vis spectra of the dried catalyst precursors.

Table 2
Parameters resulting from the fit of Mo K-edge Fourier filtered k^2 weighted EXAFS function of the CoMoP impregnation solution (Δk = 4.8–16.5 Å^{-1}, ΔR = 0.5– 4 Å)[a]

Shell	N (±10%)	R (Å) (±1%)	$\Delta\sigma^2$ (10^{-3} Å^2) (±5%)	ΔE_0 (eV) (±10%)
O1	2.1	1.71	1.2	−1.7
O2	2.1	1.95	2.5	−10.1
O3	2.0	2.36	9.1	−2.0
Mo	2.3	3.42	2.2	−3.0
P	2.0	3.50	−1.6	1.0

[a] k^2 variance (%) Im. = 1.4, Abs. = 0.5, goodness of fit = 0.06.

observed in the spectrum of ammonium heptamolybdate (not shown here), where molybdenum is octahedrically coordinated by oxygen ions. However, in the spectrum of CoMoP-TEG-DME/γ-Al_2O_3 the signal at 325 nm is weak, and in the spectra of the CoMoP_std/γ-Al_2O_3 and the CoMoP/γ-Al_2O_3 samples it is absent. This suggests that in the absence of glycols the molybdenum is mainly in a tetrahedral geometry. A broad band between 500 and 600 nm is clearly visible for the CoMoP/γ-Al_2O_3 and the CoMoP/SiO_2 samples. This band is typical for cobalt in a octahedral geometry. However, in the case of the CoMoP-TEG/γ-Al_2O_3 and CoMoP/γ-Al_2O_3 + TEG samples, this band is hidden by a much broader band between 700 and 800 nm. The UV spectrum of the fresh γ-Al_2O_3 + TEG sample revealed that this band arises from the glycol.

3.3.2. Mo X-ray absorption of the CoMoP impregnation solution and the CoMoP/SiO_2 and CoMoP/γ-A_2O_3 + TEG catalyst precursors

To study the interaction of the phosphomolybdate species with γ-Al_2O_3 and how it is affected by the glycol, we compared the Fourier transform functions of the EXAFS spectra measured at the Mo K-edge of the CoMoP impregnation solution and of the CoMoP/SiO_2 and CoMoP/γ-Al_2O_3 + TEG catalyst precursors. The k^3-weighted Fourier transforms (magnitude and imaginary part of the transform) of the CoMoP impregnation solution and CoMoP/SiO_2 sample are compared in Fig. 7, whereas Fig. 8 shows a comparison between the k^3-weighted Fourier transforms (magnitude and imaginary part of the transform) of the CoMoP/SiO_2 and the CoMoP/γ-Al_2O_3 + TEG samples. Fig. 7 shows that the

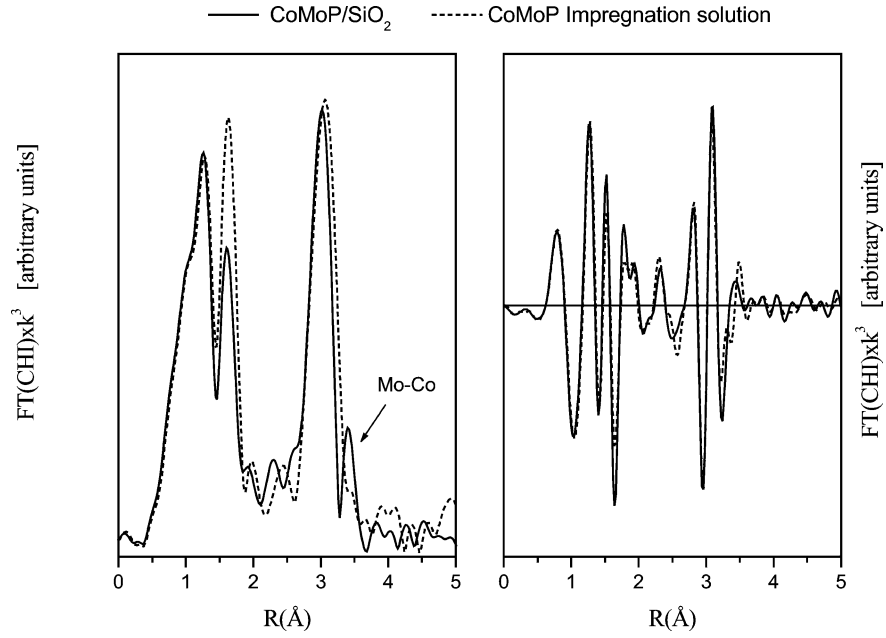

Fig. 7. Mo K-edge k^3-weighted EXAFS absolute and imaginary part of the Fourier transforms of dried CoMoP/SiO_2 (solid) and CoMoP impregnation solution (dashed).

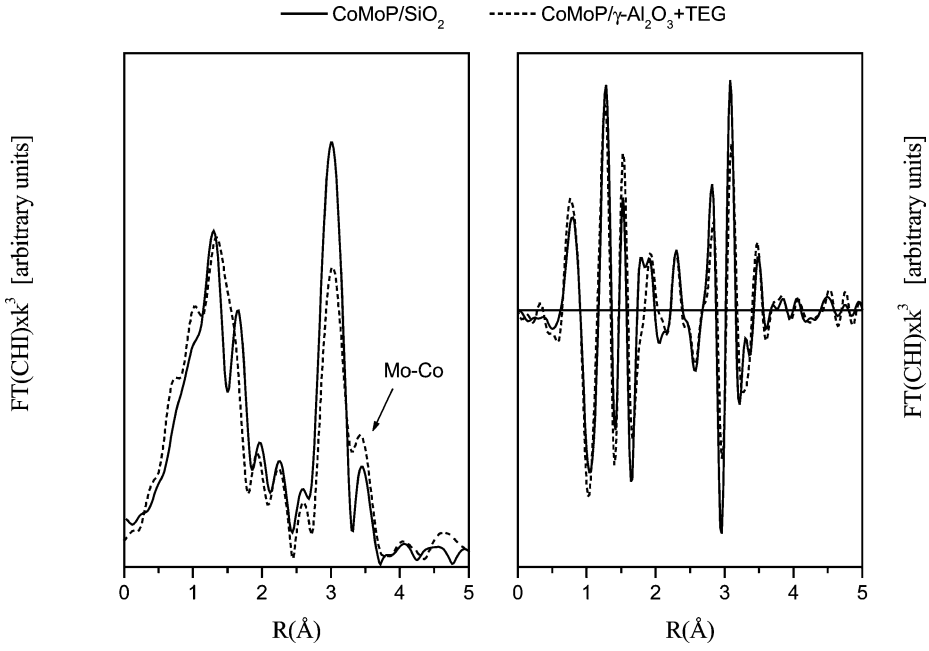

Fig. 8. Mo K-edge k^3-weighted EXAFS absolute and imaginary part of the Fourier transforms of the CoMoP/SiO_2 (solid) and the dried CoMoP/γ-Al_2O_3 + TEG catalyst precursors (dashed).

local environment of molybdenum in the CoMoP/SiO_2 sample hardly differed from that in the CoMoP impregnation solution. The CoMoP/γ-Al_2O_3 + TEG and CoMoP/SiO_2 samples show similar features in the region between 0.5 and 2.5 Å (Fig. 8), but the CoMoP/γ-Al_2O_3 + TEG sample shows a smaller signal between 2.5 and 3.25 Å and a more intense one between 3.25 and 4.0 Å. The results of the fits for the spectra of CoMoP/SiO_2 and CoMoP/γ-Al_2O_3 + TEG catalyst precursors are shown in Table 3.

When a silica support is used, the molybdenum environment is very similar to that of the CoMoP impregnation solution (Fig. 7). The fit results shown in Table 3 confirm that the structure of the $HP_2Mo_5O_{23}{}^{5-}$ anion was retained on the silica support. In addition, the peak at about 3.5 Å (not phase corrected) could be fitted with a Mo–Co contribution. The reference for the Co back-scatterer was calculated by the FEFF 8 code on the basis of the crystallographic data for $Na_5H(P_2Mo_5O_{23})$ [28]. In this compound each Mo^{6+} ion is

Table 3
Parameters resulting from the fit of Mo K-edge Fourier filtered k^2 weighted EXAFS function of the dried catalysts precursors

Shell	N (±10%)	R (Å) (±1%)	$\Delta\sigma^2$ (10^{-3} Å^2) (±5%)	ΔE_0 (eV) (±10%)
CoMoP/γ-Al_2O_3 + TEG[a] (Δk = 4.5–17.0 Å^{-1}, ΔR = 0.5–4.3 Å)				
O1	2.6	1.70	3.1	6.2
O2	3.0	1.94	7.8	5.3
O3	0.8	2.40	3.4	−1.8
Mo	2.1	3.42	3.5	2.5
P	2.3	3.56	1.1	4.6
Co	0.6	3.65	0.16	−8.7
CoMoP/SiO_2[b] (Δk = 4.7–18.8 Å^{-1}, ΔR = 0.5–4 Å)				
O1	2.0	1.72	1.3	0.1
O2	2.0	1.92	4.7	−2.7
O3	2.0	2.32	2.8	5.5
Mo	2.0	3.40	6.4	8.4
P	1.7	3.55	0.4	3.7
Co	1.0	3.66	5.3	−10.2

[a] k^2 variance (%): Im. = 1.8, Abs. = 0.6, goodness of fit = 0.006.
[b] k^2 variance (%): Im. = 2.8, Abs. = 1.3, goodness of fit = 0.01.

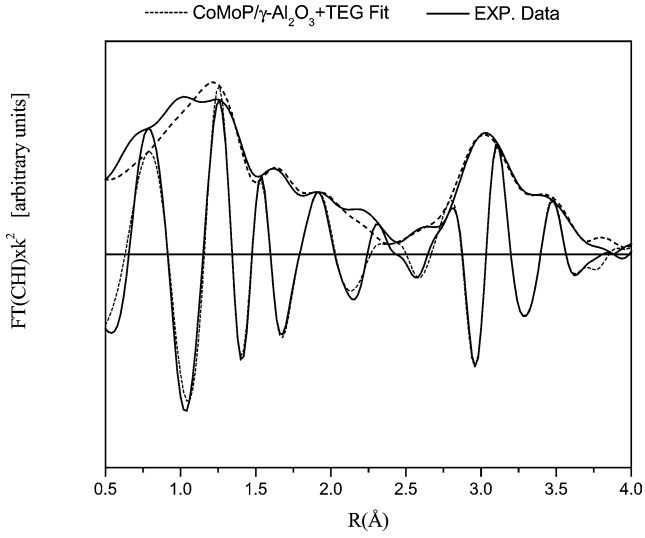

Fig. 9. Mo K-edge k^2-weighted EXAFS Fourier transforms of CoMoP/γ-Al_2O_3 + TEG, experimental (solid) and fit (dashed). Δk = 4.5–17.0 Å^{-1}, ΔR = 0.5–4.3 Å.

surrounded by two Na^+ ions at distances of 3.68 and 3.74 Å. Therefore, we calculated a reference for a Mo–Co contribution in such a way that one Co^{2+} ion replaces two Na^+ ions located 3.71 Å from the Mo^{6+}. The fit led to a Mo–Co distance of 3.66 Å.

The results of the fit for CoMoP/γ-Al_2O_3 + TEG, shown in Table 3 and Fig. 9, proved that on the γ-Al_2O_3 + TEG support the structure of the diphosphopentamolybdate was retained. Furthermore, the broad pre-edge peak in the Mo K-edge XANES spectra of Fig. 10 confirmed the octahedral geometry for the molybdenum.

3.3.3. *Mo X-ray absorption of CoMoP-TEG/γ-Al_2O_3 and CoMoP/γ-Al_2O_3*

The k^3-weighted Fourier transform EXAFS function of the CoMoP-TEG/γ-Al_2O_3 and CoMoP/γ-Al_2O_3 catalyst precursors showed that, in the presence of TEG, both the first shell (0.5–2.5 Å) and the second shell (2.5–4 Å) around Mo are affected (Fig. 11). Compared with the Fourier transform of CoMoP/γ-Al_2O_3, the Fourier transform of the CoMoP-TEG/γ-Al_2O_3 sample shows a strong decrease in intensity between 0.5 and 1.5 Å (not phase corrected). In contrast, the signal between 2.5 and 4.0 Å (not phase corrected) of

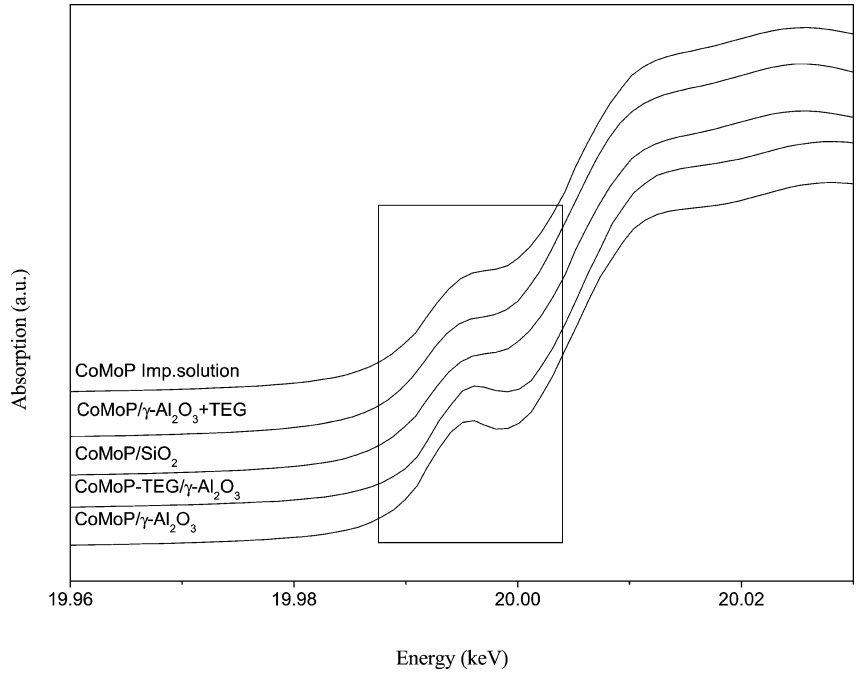

Fig. 10. Mo K-edge XANES spectra of the CoMoP impregnation solution, dried CoMoP/γ-Al_2O_3 + TEG, CoMoP/SiO_2, and CoMoP/γ-Al_2O_3 with and without TEG.

CoMoP-TEG/γ-Al_2O_3 is much more intense and asymmetrical than that of CoMoP/γ-Al_2O_3.

In CoMoP/γ-Al_2O_3, the first shell of neighboring atoms was fitted with two O atoms at 1.68 Å and two at 2.37 Å (Table 4). This suggests that, on average, the molybdenum is in a distorted tetrahedral geometry. This molybdenum geometry in the CoMoP/γ-Al_2O_3 sample was confirmed by the Mo K-edge XANES shown in Fig. 10. The pre-edge peak is assigned to the 1s → 4d electronic transition, which is only allowed in a tetrahedral or distorted octahedral environment [32,33].

Table 4
Parameters resulting from the fit of Mo K-edge Fourier filtered k^2 weighted EXAFS function of the dried catalysts precursors

Shell	N (±10%)	R (Å) (±1%)	$\Delta\sigma^2$ (10^{-3} Å^2) (±5%)	ΔE_0 (eV) (±10%)
CoMoP/γ-Al_2O_3[a] ($\Delta k = 3.8$–13.6 Å^{-1}, $\Delta R = 0.5$–4.0 Å)				
O1	2.3	1.68	4.2	9.5
O2	1.6	2.37	5.5	−9.5
Al1	1.1	3.40	4.7	8.1
Al2	2.3	3.73	6.3	0.4
CoMoP-TEG/γ-Al_2O_3[b] ($\Delta k = 4$–15.8 Å^{-1}, $\Delta R = 0.5$–4.0 Å)				
O1	2.0	1.71	4.2	−3.4
O2	1.2	1.90	8.0	−5.5
O3	2.3	2.35	6.0	−0.2
Mo	2.3	3.43	2.6	−10.0
P	2.0	3.55	0.1	−5.5
Co	1.0	3.87	3.7	1.1

[a] k^2 variance (%): Im. = 1.0, Abs. = 0.4, goodness of fit = 0.02.
[b] k^2 variance (%): Im. = 1.3, Abs. = 0.5, goodness of fit = 0.004.

The signal at 3.25 Å (not phase corrected) in the Fourier transform of CoMoP/γ-Al_2O_3 is much weaker than that of CoMoP-TEG/γ-Al_2O_3 at 3.0 Å (Fig. 11). The fit for CoMoP/γ-Al_2O_3 indicated that one Al atom at 3.40 and two Al atoms at 3.73 Å are responsible for the signal between 3 and 4 Å in the Fourier transform. The reference for the Al shell was calculated from the FEFF 8 code based on the crystallographic data of $LiAl(MoO_4)_2$ [34]. In this structure, molybdenum is tetrahedrally surrounded by four oxygen atoms at about 1.7 Å and three Al atoms at 3.45, 3.58, and 3.64 Å. The F-test proved that this model had an 85% chance to describe the CoMoP/γ-Al_2O_3 better than other attempted models. It has to be stressed that the crystallographic data refer to a bulk $LiAl(MoO_4)_2$ sample, whereas our results arise from a molybdate supported on alumina. This may explain the larger distance observed for the two Al atoms at 3.73 Å that arise from the linkage of the MoO_4^{2-} anions to the aluminum atoms of the support.

The results of the fit for CoMoP-TEG/γ-Al_2O_3 are shown in Table 4 and Fig. 12. The first shell around the Mo atom is composed of three O contributions at 1.71, 1.90, and 2.35 Å. The UV–vis spectrum for this sample suggested that molybdenum may be in both octahedral and tetrahedral coordination. As a *bulk* technique, EXAFS cannot distinguish between the two different states of molybdenum; it gives information only on the average structure. Therefore, an average structure of molybdenum with five oxygen atoms in the first coordination sphere, as suggested by the results of the fit, is in good agreement with the UV–vis measurements. The very broad pre-edge peak in the Mo K-edge XANES spectra of CoMoP-TEG/γ-Al_2O_3 (Fig. 10) indicates that the 1s → 4d electronic transition is only slightly

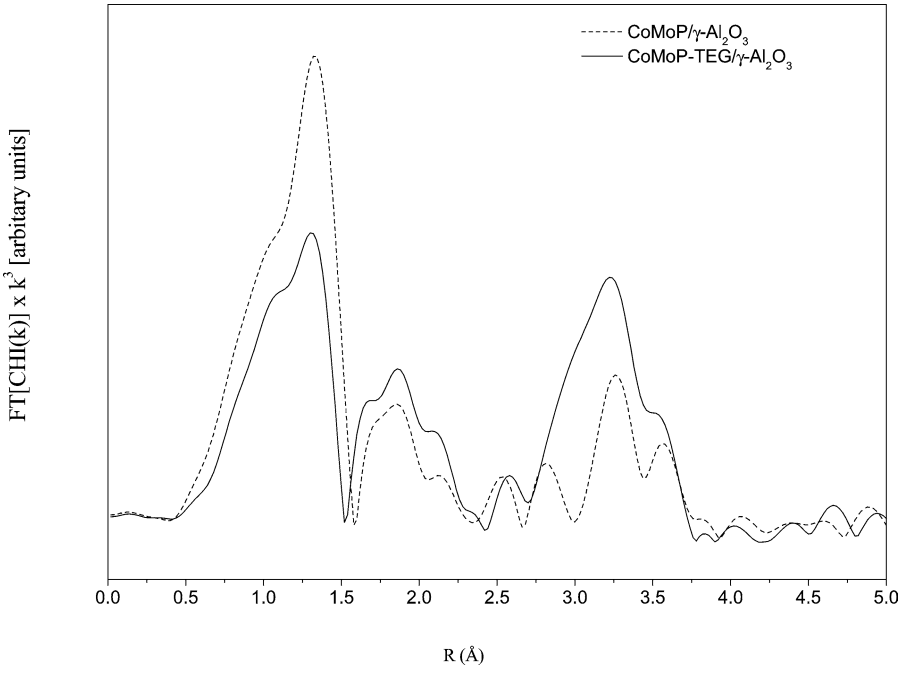

Fig. 11. Mo K-edge k^3-weighted EXAFS Fourier transforms of dried CoMoP-TEG/γ-Al_2O_3 (solid) and CoMoP/γ-Al_2O_3 (dashed).

allowed because of a strong distortion of the Mo octahedrons [32]. The second shell of neighboring atoms could be fitted with a Mo–Mo contribution at 3.43 Å and a Mo–P contribution at 3.55 Å. Furthermore, the shoulder at about 3.5 Å (not phase corrected) could be fitted with a Mo–Co contribution at 3.86 Å. This contribution was confirmed by application of the phase correction to the EXAFS Fourier transform with the calculated Mo–Co reference [17]. With this technique, the Mo–Co contribution was clearly separated from the Mo–Mo and Mo–P contributions, as shown in the k^1 and k^3 difference files in Fig. 13.

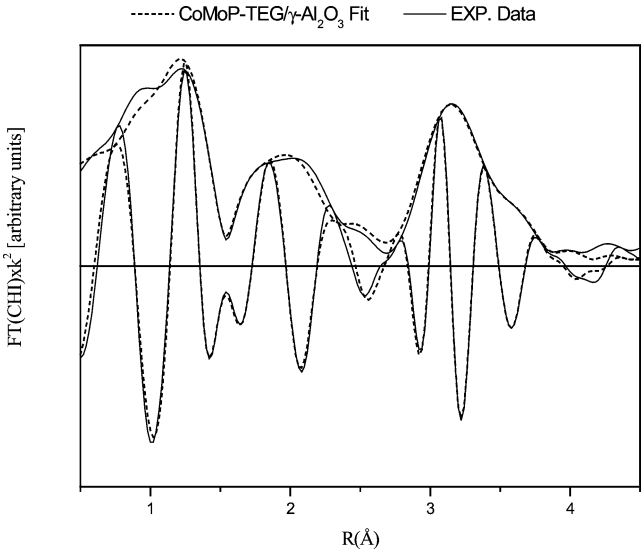

Fig. 12. Mo K-edge k^2-weighted EXAFS Fourier transforms of CoMoP-TEG/γ-Al_2O_3, experimental (solid) and fit (dashed). $\Delta k = 4.0$–15.8 Å^{-1}, $\Delta R = 0.5$–4 Å.

3.3.4. DRIFT spectra

The interaction of glycol with the support was studied by impregnating γ-Al_2O_3 and SiO_2 with an aqueous solution of TEG, EG, and TEG-DME. Fig. 14 shows FTIR spectra for γ-Al_2O_3 + TEG, γ-Al_2O_3 + EG, γ-Al_2O_3 + TEG-DME, SiO_2 + TEG-DME, SiO_2 + TEG, bare γ-Al_2O_3, and SiO_2. All of the glycol-containing samples showed a broad signal between 3000 and 2750 cm^{-1}, which is due to the –CH_2–, –C_2H_4–, and –CH_3– vibrations. The peak at about 1650 cm^{-1} is very intense in both the γ-Al_2O_3 + TEG and γ-Al_2O_3 + EG samples and is typical for an Al–O–C vibration [35]. However, the SiO_2 + TEG sample did not show this feature. These results suggests that TEG and EG interact more strongly with the alumina surface than with the silica surface. Moreover, the absence of the Al–O–C vibration in the spectra of the γ-Al_2O_3 + TEG-DME and SiO_2 + TEG-DME samples suggests that TEG and EG react strongly with the alumina surface by means of OH groups. Since it is known that the OH groups of silica are mainly acidic [36], both TEG and EG probably replace the basic OH groups of the alumina with subsequent release of water. However, we cannot exclude the possibility that they also interact with the coordinative unsaturated (C.U.) aluminum sites, although only a few C.U. sites are present on the alumina surface [37].

4. Discussion

In this section, we first consider the structure of phosphomolybdate anions in the impregnation solution in the presence and absence of TEG. Then we analyze the effect of TEG and the support on the adsorption of the phosphomolybdate clusters. These effects will be correlated with the

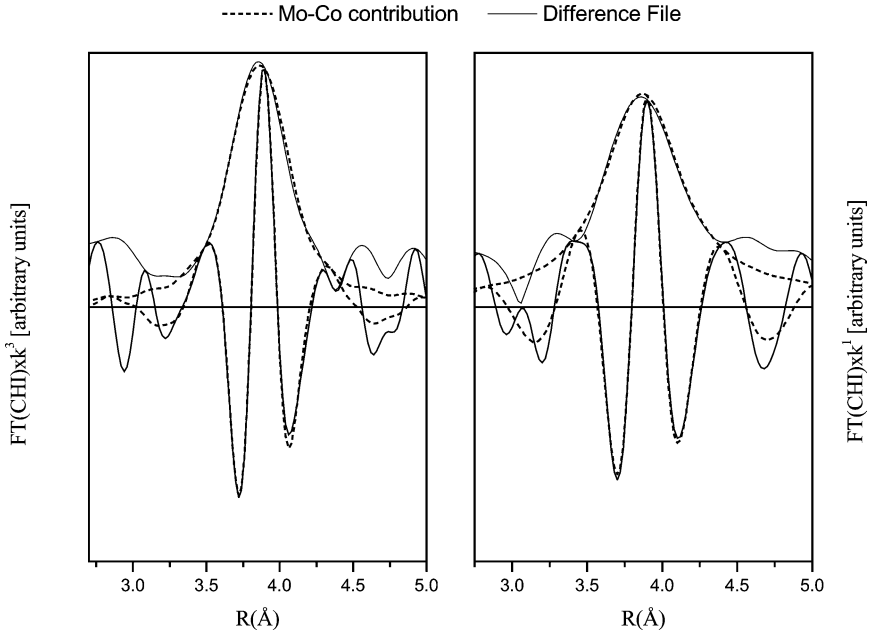

Fig. 13. k^1 (right) and k^3 (left) weighted EXAFS Fourier transforms of the fitted Mo–Co contribution in dried CoMoP-TEG/γ-Al_2O_3, experimental (dashed) and difference file (solid).

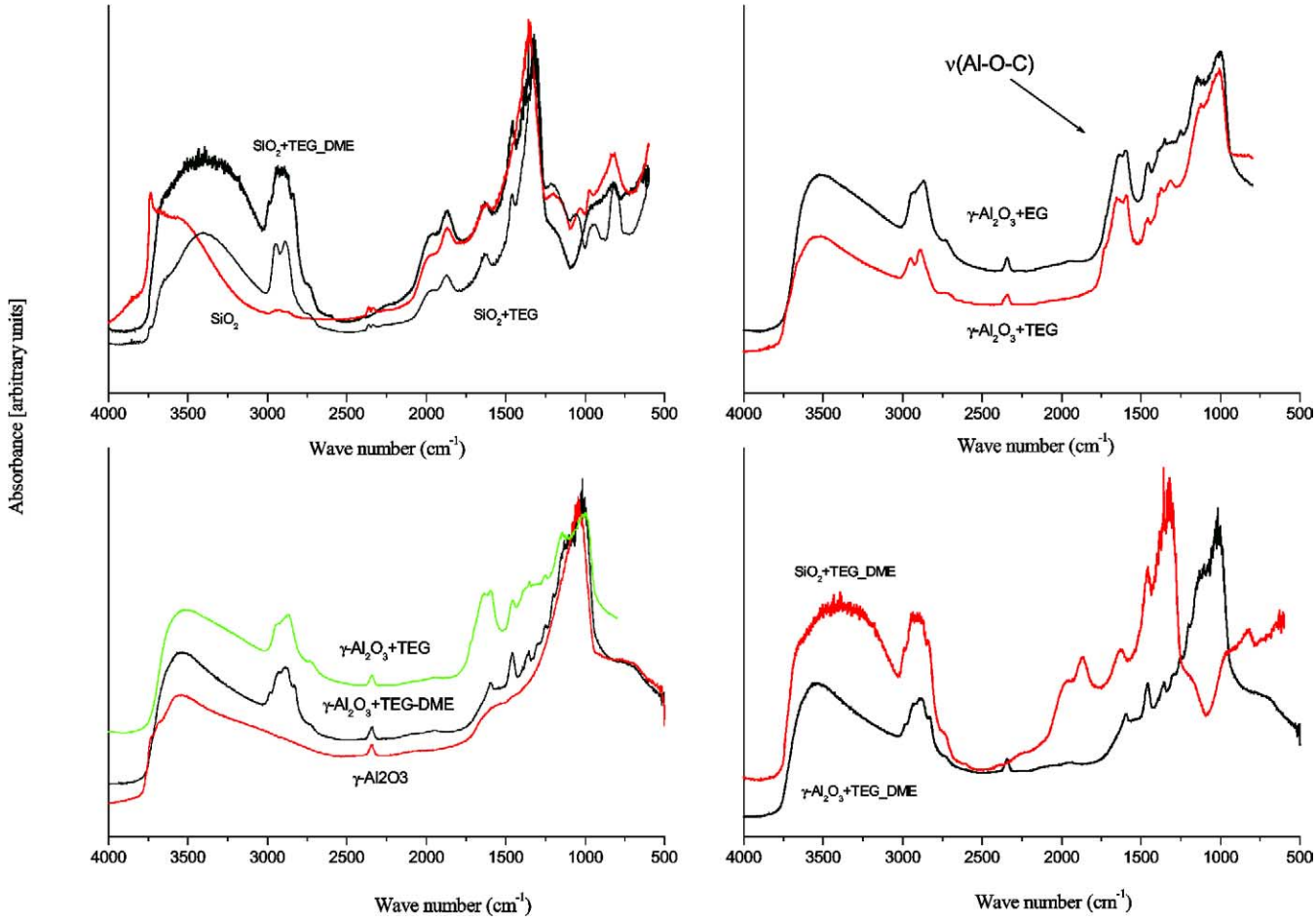

Fig. 14. IR spectra of dried SiO_2 + TEG-DME, SiO_2 + TEG, γ-Al_2O_3 + TEG-DME, γ-Al_2O_3 + TEG, γ-Al_2O_3 + EG, SiO_2, and γ-Al_2O_3 powders.

catalytic performance of the CoMoP-TEG/γ-Al_2O_3 sample.

4.1. The impregnation solution

Pettersson et al. [4,5] observed that $H_xP_2Mo_5O_{23}^{(6-x)-}$ anions are present in an acidic solution with a P/Mo molar ratio of 0.4. Our analysis of the CoMoP and CoMoP-TEG impregnation solutions by laser Raman spectroscopy, ^{31}P NMR, and Mo *K*-edge EXAFS confirmed that molybdenum trioxide and phosphoric acid react stoichiometrically in aqueous solution to the $HP_2Mo_5O_{23}^{5-}$ anion. Because of the acidity of the resulting solution, the $CoCO_3$ added after the dissolution of the MoO_3 dissolved completely, and CO_2 evolved. The paramagnetic effect of cobalt on the ^{31}P NMR spectra of both impregnation solutions demonstrates that cobalt and phosphorus are in close proximity [26]. The formation of insoluble $Co_3(PO_4)_2$ was avoided by the addition of the cobalt salt after the formation of $HP_2Mo_5O_{23}^{5-}$. The ^{31}P NMR paramagnetic effect suggests that the Co^{2+} cations are in solution as the counter-ions of the $HP_2Mo_5O_{23}^{5-}$ anions, forming the $Co_xHP_2Mo_5O_{23}^{(5-2x)-}$ complex. Griboval et al. reported that the diphosphopentamolybdate anion, as an irreducible species, is vulnerable to complex cobalt cations in the impregnation solution [6,7]. ^{13}C NMR measurements of the CoMoP-TEG impregnation solution showed three sharp peaks at 60.6, 70, and 72 ppm arising for the three different types of carbon atoms in TEG. The absence of a paramagnetic effect showed that TEG did not form a chelate complex with the Co^{2+} ions. Such a behavior was expected because TEG is a weak chelating ligand. The analysis of the Mo *K*-edge EXAFS of the CoMoP solution confirmed the presence of $HP_2Mo_5O_{23}^{5-}$, but no Mo–Co contribution was found. EXAFS measurements of solutions normally show higher Debye–Waller factors than did those of solid samples [20] because of the inhomogeneous spread of the distances. This leads to a broadening of the signal of the Mo–Co contribution in the Fourier transform of the EXAFS function. At high *R* values, these effects make the fit of a Mo–Co contribution impossible.

4.2. The CoMoP/γ-Al_2O_3 and CoMoP/SiO_2 dried catalyst precursors

The impregnation of the metal precursor on the support is a crucial step in the preparation of the supported catalysts, and it depends on several factors. The alumina and silica surfaces possess different types of surface OH groups. SiO_2

contains mainly acidic and γ-Al_2O_3 both basic and acidic OH groups. Moreover, γ-Al_2O_3 exposes coordinatively unsaturated (C.U.) Al^{3+} sites, which are absent on the SiO_2 support. One consequence of these different OH groups is the different point of zero charge (PZC) of these supports. The PZC is the pH value at which the surface of the support is electrically neutral. γ-Al_2O_3 has a PZC of about 8 and SiO_2 a PZC of about 2. Such a difference in the PZC strongly affects the chemistry that takes place during the impregnation of the catalyst precursor, especially when the metal precursor species in the impregnation solution depend on pH-sensitive chemical equilibria. This is the case when phosphomolybdates are used as precursors for molybdenum. As shown above, $HP_2Mo_5O_{23}^{5-}$ species are present in the CoMoP impregnation solution. According to Pettersson et al. this species is stable up to pH 6 [4]. When the impregnation solution comes in contact with the γ-Al_2O_3 surface, the pH of the solution rises. When the pH rises above 6 the $HP_2Mo_5O_{23}^{5-}$ species start to decompose into phosphate and molybdate [38]. The released phosphate reacts with the acidic Al–OH groups to form $AlPO_4$, the presence of which is detected by MAS ^{31}P NMR experiments (not shown here); the molybdate species adsorb first to basic Al–OH and Al^{3+}. When both basic Al–OH and Al^{3+} sites are fully occupied, the molybdate starts to react with P–OH groups of the $AlPO_4$ as well. The coordination of molybdenum is tetrahedral (as a monolayer of monomolybdate) for a low Mo loading (up to 12%) or octahedral (as octamolybdate) for a high Mo loading [39]. UV–vis and Mo *K*-edge XAFS measurements showed that in the CoMoP/γ-Al_2O_3 sample the molybdenum is mainly tetrahedrally coordinated, forming an "interaction species" with the alumina surface similar to that proposed by Desikan et al. for an uncalcined MoO_3/γ-Al_2O_3 sample [40]. As far as the cobalt is concerned, in the CoMoP/γ-Al_2O_3 sample it probably adsorbs to the $AlPO_4$, forming a species that resembles $Co_3(PO_4)_2$ [41]. When SiO_2 was used as a support, the molybdenum was mainly octahedrally coordinated and the EXAFS results showed that the local structure of molybdenum resembles that of the $HP_2Mo_5O_{23}^{5-}$ anion. Moreover, the Mo–Co contribution at 3.66 Å suggested that Mo and Co are in close proximity. Thus, it is evident that the final structure of the molybdenum precursor strongly depends on the support.

4.3. The CoMoP-TEG/γ-Al_2O_3 and the CoMoP/γ-Al_2O_3 + TEG dried catalyst precursor: the role of TEG

It was much more complicated to elucidate the molybdenum structure in the presence than in the absence of TEG. The UV–vis measurements carried out on CoMoP-TEG/γ-Al_2O_3 showed that molybdenum is present in both tetrahedral and octahedral geometry. This was suggested by the EXAFS analysis as well. The Mo–P contribution at 3.55 Å suggests that the structure of the diphosphopentamolybdate species was retained to a certain extent; therefore the octahedral molybdenum arises from the diphosphopentamolybdate-like species. On the other hand, our EXAFS results showed that when TEG is adsorbed first on the γ-Al_2O_3, the decomposition of the diphosphopentamolybdate is prevented. Obviously, the glycol was responsible for this effect. The DRIFT measurements of the γ-Al_2O_3 + TEG showed a signal corresponding to an Al–O–C vibration [36], suggesting that there was a strong interaction between the alumina support and the glycol. Such an interaction was not observed for SiO_2 + TEG. The DRIFT experiments carried out on samples treated with TEG-DME did not show any strong interaction with the alumina support. However, samples treated with EG showed a strong signal corresponding to the Al–O–C vibration. This proved that glycol can strongly interact with the alumina surface by means of the OH groups. Apparently, the OH groups of TEG react with the basic OH groups of the alumina surface, releasing water and forming an Al–O–C bond. We cannot exclude the possibility that the glycol interacted with the Al^{3+} C.U. sites as well. When basic OH and Al^{3+} sites are blocked by glycol, the interaction between the diphosphopentamolybdate species and γ-Al_2O_3 is affected. Furthermore, because of the alumina–glycol interaction, the PZC of the alumina changes and the decomposition of the diphosphopentamolybdate is diminished. However, at the beginning of the impregnation, when both the basic OH groups and the Al^{3+} sites are fully available on the alumina support, glycol and diphosphopentamolybdate anions compete for the same adsorption sites. Although the strength of interaction with the alumina sites is larger for diphosphopentamolybdate than for glycol, the adsorption of the latter will be favored for two reasons. First, the glycol concentration in the impregnation solution is about four times higher than that of diphosphopentamolybdate. Second, the adsorption of glycol on the alumina sites takes place without reconstruction, whereas the adsorption of diphosphopentamolybdate requires the decomposition of the cluster followed by adsorption of the resulting phosphate and molybdate on the alumina sites. However, those diphosphopentamolybdate clusters that reach the alumina adsorption sites earlier than glycol decompose and lead to tetrahedrally coordinated molybdenum. On the other hand, when glycol adsorbs first, it prevents the decomposition of the diphosphopentamolybdate species with the alumina surface. This explains the tetrahedral/octahedral mixture for the molybdenum coordination observed in the CoMoP-TEG/γ-Al_2O_3 catalyst precursor. When glycol is adsorbed to the support first, this competition is eliminated, allowing the diphosphopentamolybdate species to precipitate in the pores of the γ-Al_2O_3 + TEG support as a cobalt salt.

4.4. Catalytic activity

The phosphate anion can be considered to be one of the most effective additives of alumina-based Mo-containing hydrotreating catalysts. The activity tests showed that all alumina-supported catalysts doped with phosphate had a higher activity than the CoMo and CoMo-TEG catalysts

prepared according to the standard route. Exhaustive reviews of the influence of phosphorus and phosphate on the properties of alumina-based catalyst were recently published [42,43]. The positive effect on the catalysts induced by these additives is due to a combination of factors. Phosphate strongly interacts with alumina adsorption sites, with which the molybdate can strongly interact. As a consequence, in the presence of phosphate the molybdate will be present predominantly as a polyanion, which can be better sulfided than the monoanion. Moreover, Co^{2+} also interacts more weakly with the alumina, becoming easier to sulfide and forming more Co atoms along the edges of the MoS_2 slabs. Another important effect caused by the weakening of the interaction of the molybdate with the alumina surface is the increase in the stacking of MoS_2 and thus the formation of the more active type II Co–Mo–S structure.

Despite the presence of TEG, the CoMo-TEG/γ-Al_2O_3 catalyst hardly showed an improvement in activity with respect to the CoMo/γ-Al_2O_3 sample. However, when TEG (or EG) is added to the CoMoP and the CoMoP-std impregnation solution, an increase in the HDS activity of the resulting catalyst was observed. The activity of the CoMoP-TEG_std/γ-Al_2O_3 was not as high as that of the CoMoP-TEG/γ-Al_2O_3 sample. An attempt to explain this result is mentioned further in the text, and it is related to NH_4^+ ions, which are present in the CoMoP_ std impregnation solution but are missing in the CoMoP-TEG solution.

The CoMoP/γ-Al_2O_3 + TEG catalyst showed a lower activity than the CoMoP/γ-Al_2O_3 and CoMoP-TEG/γ-Al_2O_3 catalysts. This may arise from the different morphology of the γ-Al_2O_3 + TEG surface. This support showed a lower BET surface area and a smaller pore volume; moreover, the double impregnation carried out for the preparation of this catalyst may have led to a poorer dispersion of the catalyst. This will be confirmed by XPS experiments. The activity of the CoMoP-TEG-DME/γ-Al_2O_3 catalyst was lower because strong interaction with the support was not achieved, and it was even lower than the activity of CoMoP/γ-Al_2O_3 because of the lower phosphate loading. The silica-based catalysts showed a very poor activity. This can be explained by taking into account the very low PZC of SiO_2. The pH of the impregnating solution was not low enough to charge the silica surface positively. Therefore, because of electrostatic repulsion, the phosphomolybdate anion may not spread uniformly over the silica surface, thus leading to a very poor dispersion.

Griboval et al. showed that catalysts containing irreducible Keggin-type phosphomolybdate anions possess a higher Co/Mo atomic ratio and form $Co_{3.5}PMo_{12}O_{40}$. This compound leads to a better decoration of the metal promoter on the MoS_2 phase and therefore to a higher catalytic activity [6,7]. The ^{31}P NMR spectra of the CoMoP and CoMoP-TEG impregnation solutions showed a strong P–Co interaction. Moreover, the EXAFS results for CoMoP/SiO_2 and CoMoP/γ-Al_2O_3 + TEG suggest that cobalt functions as a counter-cation for a diphosphopentamolybdate-like species in which Co and Mo are in close proximity, with a higher Co/Mo atomic ratio. As mentioned above, this feature leads to a better decoration of the MoS_2 cluster. The NH_4^+ cations in the CoMoP-TEG_std impregnation solution, however, may compete with Co^{2+}, thus lowering the Co/Mo atomic ratio of the oxidic catalytic precursors. This could explain the lower activity of CoMoP-TEG_std/γ-Al_2O_3 with respect to CoMoP-TEG/γ-Al_2O_3. ^{31}P NMR experiments are in progress to prove this theory. When a bare γ-Al_2O_3 support is used, despite the high overall Co/Mo atomic ratio, the local Co/Mo ratio cannot be maintained because the diphosphopentamolybdate species strongly interact with the γ-Al_2O_3 support and decompose. The use of TEG prevents the decomposition of the diphosphopentamolybdate species. Therefore, in the CoMoP-TEG/γ-Al_2O_3 sample, the Co/Mo atomic ratio is also locally much higher and the promoting effect is improved.

The role of TEG can be viewed as forming a layer between the metal precursors and the alumina surface. In this way, TEG induces the metal precursors to agglomerate into large islands over the alumina surface, which is modified by TEG with a high Co/Mo atomic ratio. During the sulfidation, TEG thermally decomposes beneath the metal particles, which eventually are sulfided. This process may cause cracks and ruptures of the metal-precursor islands, thus leading to redispersion. The TGA analysis showed that a strong weight loss at about 250 °C occurred only for the TEG-containing samples. This was ascribed to the thermal decomposition of TEG, which was also confirmed by in situ DRIFT experiments on the γ-Al_2O_3 + TEG sample with heating at 300 °C. We observed that the signal corresponding to the Al–O–C vibration disappeared at about 250 °C.

Recently, van Dillen et al. proposed that the more viscous the impregnation solution is, the more the catalyst becomes dispersed on the surface of the support [44]. As glycol makes the solution more viscous it can lead to a better dispersion of the catalytic sites on the support, thus increasing the catalytic activity.

We have to consider, however, that the thermal response of a catalyst depends also on the structure of the active phase. Therefore, performing the same catalytic test, even on catalysts with the same chemical composition but different structure, may lead to slightly different trends in the ranking of the obtained catalytic activities. To confirm our reported ranking, HDS experiments with thiophene should be performed at different temperatures.

5. Conclusions

The use of glycol allowed the preparation of more active CoMo hydrotreating catalysts prepared by the dissolving of H_3PO_4, MoO_3, $CoCO_3$, and glycol in water. H_3PO_4 reacts stoichiometrically with MoO_3 and forms diphosphopentamolybdate species, and $CoCO_3$ dissolves completely and probably forms a heteropolymolybdate with a high Co/Mo

atomic ratio. The glycol does not interact with metal precursors in the impregnation solution. The main role of the glycol is achieved during the impregnation of the support. By reacting with the basic Al–OH and Al^{3+} surface sites of the γ-Al_2O_3 support, glycol hinders the interaction between the cobalt-diphosphomolybdate species and the γ-Al_2O_3 support. In this way the glycol favors the formation of oxidic clusters with a very high Co/Mo atomic ratio. As a consequence, more Co atoms are available to promote the MoS_2 crystallites formed upon sulfidation. During the thermal decomposition of the glycol, the catalytic sites may undergo a redispersion. However, the exact nature of the oxidic catalytic precursors is not clearly defined yet. XPS and laser Raman experiments with the oxidic catalyst are in progress to fully define the structure of the adsorbed metal precursors.

Acknowledgments

The authors thank the Swiss-Norwegian Beamline staff for assistance during EXAFS measurements at ESRF (Grenoble, France) and Marco Luechinger for the nitrogen adsorption measurements and AAS analysis. This project was supported by the Swiss National Science Foundation.

References

[1] E. Yamaguchi, Y. Uragami, H. Yokozuka, K. Uekusa, T. Yamaguchi, S. Abe, T. Kamo, T. Suzuki, European Patent Application 0601722 B 1 (1998) Sumitomo Metal.
[2] M. Jian, J.L.R. Cerda, R. Prins, Bull. Soc. Chim. Belg. 104 (1995) 225.
[3] C.W. Fitz, H.F. Rase, Ind. Eng. Chem. Prod. Res. Dev. 22 (1983) 40.
[4] L. Pettersson, I. Andersson, L.O. Ohman, Acta Chem. Scand. A 39 (1985) 53.
[5] L. Pettersson, I. Andersson, L.O. Ohman, Inorg. Chem. 25 (1986) 4726.
[6] A. Griboval, P. Blanchard, E. Payen, M. Fournier, J.L. Dubois, Stud. Surf. Sci. Catal. 1061 (1997) 81.
[7] A. Griboval, P. Blanchard, E. Payen, M. Fournier, J.L. Dubois, Catal. Today 45 (1998) 277.
[8] J.A.R. van Veen, P.A.J.M. Hendriks, E.J.G.M. Romers, R.R. Andrea, J. Phys. Chem. 94 (1990) 5282.
[9] W.C. Cheng, N.P. Luthra, J. Catal. 109 (1988) 163.
[10] M.S. Thompson, European patent application 01181035 A2 (1986).
[11] R. Cattaneo, T. Shido, R. Prins, J. Catal. 185 (1999) 199.
[12] R. Cattaneo, F. Rota, R. Prins, J. Catal. 199 (2001) 318.
[13] L. Medici, R. Prins, J. Catal. 163 (1996) 28.
[14] S.P.A. Louwers, R. Prins, J. Catal. 133 (1992) 94.
[15] F.W.H. Kampers, T.M.J. Maas, J. van Grondelle, P. Brinkgreve, D.C. Koningsberger, Rev. Sci. Instrum. 60 (1989) 2635.
[16] P.S. Kirlin, F.B.M. van Zon, D.C. Koningsberger, B.C. Gates, J. Phys. Chem. 94 (1990) 8439.
[17] D.C. Koningsberger, B.L. Mojet, G.E. van Dorssen, D.E. Ramaker, Topics Catal. 10 (2000) 143.
[18] S.I. Zabinsky, J.J. Rehr, A. Ankudinov, R.C. Albers, M.J. Eller, Phys. Rev. B 52 (1995) 2995.
[19] W.L. Dhandapani, S.T. Oyama, Chem. Lett. (1998) 207.
[20] M. Tromp, J.A. van Bokhoven, A.M. Arink, J.H. Bitter, G. van Koten, D.C. Koningsberger, Chem.-Eur. J. 8 (2002) 5667.
[21] J. de Graaf, A.J. van Dillen, K.P. de Jong, D.C. Koningsberger, J. Catal. 203 (2001) 307.
[22] D.C. Koningsberger, Jpn. J. Appl. Phys. 32 (1993) 877.
[23] L. Lyhamn, L. Pettersson, Chem. Scripta 12 (1977) 142.
[24] L. Pettersson, I. Andersson, L.O. Ohman, Inorg. Chem. 25 (1986) 4726.
[25] L. Canesson, A. Tuel, Chem. Commun. 2 (1997) 241.
[26] M.N. Harris, C.M. Bertolucci, L.J. Ming, Inorg. Chem. 41 (2002) 5582.
[27] J.A.R. van Veen, O. Sudmeijer, C.A. Emeis, H. de Wit, J. Chem. Soc. D alton (1986) 1825.
[28] B. Hedman, R. Strandberg, Act. Cryst. B 35 (1979) 278.
[29] M. Fournier, C. Louis, M. Che, P. Chaquin, D. Masure, J. Catal. 119 (1989) 400.
[30] C.C. Williams, J.G. Ekerdt, J.M. Jehng, F.D. Hardcastle, A.M. Turek, I.E. Wachs, J. Phys. Chem. 95 (1991) 8781.
[31] C.C. Williams, J.G. Ekerdt, J. Phys. Chem. 95 (1991) 8791.
[32] N.S. Chiu, S.H. Bauer, M.F.L. Johnson, J. Catal. 89 (1984) 226.
[33] D.C. Koningsberger, R. Prins, X-Ray Absorption: Principles, Applications, Techniques of EXAFS, SEXAFS and XANES, Wiley, New York, 1988.
[34] L.P. Solov'eva, S.V. Borisov, Kristall. 15 (1970) 577.
[35] J.A.R. van Veen, G. Jonkers, W.H. Hesselink, J. Chem. Soc. Farad. Trans. I 85 (1989) 389.
[36] J.A.R. van Veen, P.C. de Jong-Versloot, G.M.M. van Kessel, F.J. Fels, Thermo Chim. Acta 52 (1989) 359.
[37] J.A.R. van Veen, P.A.J.M. Hendriks, E.J.G.M. Romers, R.R. Andrea, J. Phys. Chem. 94 (1990) 5275.
[38] H. Kraus, R. Prins, J. Catal. 164 (1996) 251.
[39] N.Y. Topsøe, H. Topsøe, J. Catal. 139 (1993) 631.
[40] A.N. Desikan, S.T. Oyama, J. Chem. Farady. Trans 88 (1992) 3357.
[41] A. Griboval, R. Blanchard, E. Payen, M. Fournier, J.L. Dubois, J.R. Bernard, Appl. Catal. 217 (2001) 173.
[42] R. Iwamoto, J. Grimblot, Adv. Catal. 44 (2000) 417.
[43] M. Sun, D. Nicosia, R. Prins, Catal. Today 86 (2003) 173.
[44] A. van Dillen, R.J.A.M. Terörde, D.J. Lensveld, J.W. Geus, K.P. de Jong, J. Catal. 216 (2003) 257.